Full Electrical Parameter Estimation Method of PMLSM Considering Parameter Asymmetry Without External Excitation

Ziyu Zou, *Student Member, IEEE*, Mengfei Zheng, *Student Member, IEEE*, Yanxin Li, *Member, IEEE*, Qinfen Lu, *Senior Member, IEEE*, and Z. Q. Zhu, *Fellow, IEEE*

***Abstract*—The longitudinal end effect of permanent magnet linear synchronous machines induces parameter asymmetry, imparting time-varying, and nonlinear characteristics to the machine model. In parameter estimation, parameter asymmetry introduces additional estimated parameters and results in nonlinearity and coupling among the parameters. To enhance the modeling precision and estimation performance, this article proposes a full electrical parameter estimation method considering asymmetry. First, the universal asymmetric equations are formulated for modeling parameter asymmetry. After these equations are subjected to reparameterization, the linear regression formulations with model order reduction are yielded. Second, the dynamic regressor extension and mixing method is employed to achieve full parameter estimation. The quasi-steady state caused by the end effect ensures that the estimation equations incorporate sufficient excitation, thereby meeting the stability conditions without the necessity of external excitation. Finally, the comparative, disturbance, and control application experiments are carried out, which validate the effectiveness and merits of the estimation method.**

***Index Terms*—Dynamic regressor extension and mixing (DREM), longitudinal end effect, parameter asymmetry, para meter estimation, permanent magnet linear synchronous machine (PMLSM).**

I. Introduction

PERMANENT magnet linear synchronous machines (PMLSMs) have the advantages of direct drive, high precision, and high efficiency [1], [2], [3]. Thus, they have garnered significant attention in various applications, particularly in situations demanding high precision. To meet the demands of precise control, accurate machine models and their corresponding parameters are required, which can be obtained through parameter estimation methods. However, the PMLSMs exhibit longitudinal end effect due to their linear structure [4]. The end effect gives rise to the detent force and parameter asymmetry, both of which introduce additional disturbances [5]. In particular, the parameter asymmetry leads to modeling errors and electromagnetic thrust ripples, which affect both parameter estimation and control performance.

To mitigate the impact of asymmetry in machine control, existing research incorporates the consideration of parameter asymmetry into various controls methods, including current control [6], [7], direct thrust control [8], and preposition methods [9]. Thus, obtaining precise asymmetry parameters is crucial for devising and applying control methods in the presence of asymmetry. Furthermore, the time-varying and nonlinear components caused by asymmetry reduce the accuracy and stability of the estimation results when utilizing conventional methods. Therefore, it becomes essential to incorporate asymmetry parameters when modeling for PMLSMs, thereby prompting the requirement for the full electrical parameter estimation method that accounts for asymmetry. Nevertheless, there is limited consideration of parameter asymmetry in the estimation for PMLSMs. Consequently, this article aims to address this matter.

The parameter estimation can be classified into two categories, the offline and online methods. The offline estimation methods lack the ability to track real-time parameter changes, whereas the online methods are widely applied due to their simplicity and real-time capabilities [10]. For online parameter estimation, existing research utilizes methods such as recursive least squares (RLS) [11], extended Kalman filter (EKF) [12], high-frequency injection (HFI) [13], and neural network (NN) [14]. Within these methods, a common challenge is the issue of rank-deficiency [15]. Under steady-state conditions, the rank of the machine equation is two, thereby restricting the accurate estimation of only two parameters simultaneously. This issue significantly affects the implementation of full electrical parameter estimation.

To overcome the limitations imposed by rank-deficiency, many studies have proposed various approaches. An effective approach involves the injection of additional control signals.

Manuscript received 26 January 2024; revised 28 May 2024; accepted 6 July 2024. Date of publication 16 July 2024; date of current version 4 September 2024. This work was supported in part by the National Science Foundation of China under Grant NSFC52177061 and Grant NSFC52107061 and in part by the Natural Science Foundation of Zhejiang Province under Grant LZ23E070002. An earlier version of this paper was presented at the 2023 IEEE International Electric Machines & Drives Conference (IEMDC), San Francisco, CA, USA, May 15-18 [DOI: 10.1109/IEMDC55163.2023.10238931]. Recommended for publication by Associate Editor Y. A.-R. I. Mohamed. *(Corresponding authors: Yanxin Li; Qinfen Lu.)*

Ziyu Zou, Mengfei Zheng, Yanxin Li, and Qinfen Lu are with the College of Electrical Engineering, Zhejiang University, Zhejiang 310027, China (e-mail: eezouziyu@zju.edu.cn; m.z@zju.edu.cn; eeliyanxin@zju.edu.cn; luqinfen@zju.edu.cn).

Z. Q. Zhu is with the Department of Electronic and Electrical Engineering, The University of Sheffield, S1 3Jd Sheffield, U.K. (e-mail: z.q.zhu@sheffield.ac.uk).

This article has supplementary material provided by the authors and color versions of one or more figures available at https://doi.org/10.1109/TPEL.2024.3428529.

Digital Object Identifier 10.1109/TPEL.2024.3428529

In [16], through injecting high-frequency (HF) voltages and utilizing HF impedance models, the simultaneous estimation of four electrical parameters is achieved. With the injection of position offsets, the inductances and flux linkage can be effectively estimated [17]. In [18], the combination of HF injection and position-offset injection is employed to achieve multiparameter estimation. These external injection methods facilitate the estimation of more parameters, but they inevitably influence the normal operation of the machine. To avoid external injection, the switching effects of pulsewidth module (PWM) can be utilized in the estimation. In [19], the PWM switching model is developed to realize the full parameter estimation. Nevertheless, this method necessitates the inclusion of additional hardware implementation and is susceptible to measurement noise. Conducting estimation at different time scales can also help address the issue of rank deficiency, although the update rates for different parameters may vary [20].

In the aforementioned literature, the estimation methods are designed based on the symmetric model of permanent magnet synchronous machines (PMSMs). However, when considering asymmetry, coupling, and nonlinear components are introduced into the machine model. In addition, the number of parameters to be estimated increases to six, which worsens the rank deficiency issue. Thus, those estimation methods developed for PMSM are not applicable in PMLSM. To estimate full parameters for PMLSM, an asymmetric HF current model is derived to realize full parameters estimation with asymmetry parameters through HFI and RLS [21]. Unfortunately, the injection of HF voltage has an impact on the normal operation of the machine.

From alternative perspectives, the rank deficiency problem can also be interpreted as the issue of insufficient excitation. In [22], the observability and estimation conditions for different parameter combinations have been thoroughly analyzed based on the observability theory. It is observed that injecting external excitations into the machine increases the number of parameters that can be estimated. Besides, conventional estimation methods such as RLS and gradient descent method require satisfying the persistent excitation (PE) condition to achieve accurate estimation [23]. It is challenging to satisfy the PE condition required for full parameter estimation in practical applications, thereby leading to the issues of insufficient excitation and rank deficiency. Accordingly, the dynamic regressor extension and mixing (DREM) method is proposed in [24] to relax the PE condition. Besides, it exhibits advantages regarding the convergence performance [25] and has been employed in applications such as power systems [26] and robot manipulators [27]. Therefore, this method is utilized for parameter estimation in this article.

To realize full electrical parameter estimation considering asymmetry without external excitation, this article proposes an enhanced estimation method. The asymmetry model for PMLSM is established, and the reparameterization is performed to reduce order of estimation model. Then, the obtained linear regressions are dynamically expanded, and the parameters are decoupled through extension and mixing process. Finally, full parameter estimation is achieved applying the standard gradient descent method. This article conducts further research based on the conference paper [28]. In comparison to [28], this article provides a more detailed explanation of the proposed estimation method and a more profound investigation into the estimation principles. Furthermore, experimental validation was lacking in [28], whereas this article provides thorough validation experiments.

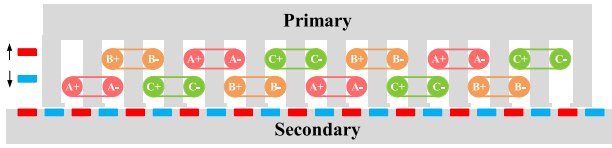

Fig. 1. Structural diagram of PMLSM prototype.

The main contribution of this article can be summarized as follows.

1) The generalized model of PMLSM considering asymmetry is established in both synchronous and stationary reference frames. Besides, the reduction of model order is performed to decrease estimation complexity.
2) All electrical parameters, including the d- and q-axis inductances, resistance, flux linkage and two asymmetry parameters are simultaneously estimated online without any external excitation. With the proposed method considering asymmetry, the estimation results exhibit enhanced estimation accuracy and stability.
3) The estimation approach and the control method are integrated to enhance control performance. The proposed method not only addresses the impact of parameter mismatches but also mitigates the disturbance caused by asymmetry in the control results.

The rest of this article is organized as follows. The asymmetry model of the PMLSM and the reparameterized linear regressions are established in Section II. In Section III, the proposed full parameter estimation method is introduced, and proofs of the stability conditions are provided. The validation experiments for comparison, robustness verification, and control applications are presented in Section IV. Finally, Section V concludes this article.

II. Model of PMLSMs Considering Asymmetry

A. PMLSM Structure and Longitudinal End Effect

The working principle of the PMLSM closely resembles that of the rotary PMSM. The structural diagram of the studied PMLSM prototype is presented in Fig. 1. It can be observed that its linear structure results in discontinuity at the ends, called longitudinal end effect. The end effect causes an unbalanced spatial distribution of the phase windings and leads to asymmetry in the inductance. Moreover, the end effect generates inherent detent force, thereby introducing additional thrust ripples.

The finite element (FE) simulation results of the inductances and the detent force for the PMLSM prototype are shown in Figs. 2 and 3. In the FE results of inductance, the ac mutual inductance of the prototype exhibits asymmetry. The asymmetry introduces modeling errors in conventional machine models based on the symmetric inductance, thereby reducing the precision and stability of estimation and control. It should be noted

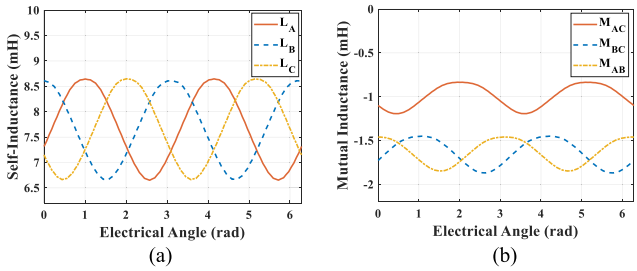

Fig. 2. FE results of inductance. (a) Self-inductance. (b) Mutual inductance.

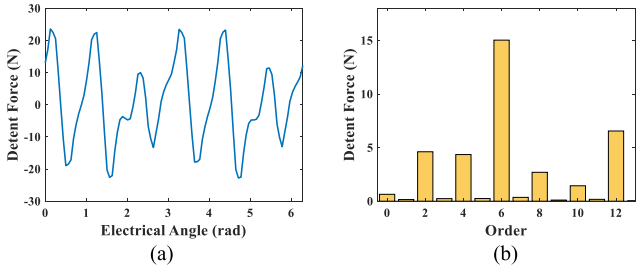

Fig. 3. FE results of the detent force. (a) Detent force. (b) Spectrum.

that this represents just one case of asymmetry, and different machine topologies may lead to various asymmetry cases. Hence, it is crucial to consider all kinds of asymmetry cases in the subsequent modeling. The FE result and the spectrum of the detent force reveal that the detent force manifests as even-order harmonic thrust ripples. And this serves as the foundation for the stability analysis.

B. Asymmetry Model

To mitigate the impact of asymmetry parameters on machine performance, the generalized machine model that accounts for inductance asymmetry is developed. To model the asymmetry of inductance, the asymmetric component is denoted by δ. The expression for the inductance of the asymmetric phase can be formulated as

$$L_{ij} = L_{sij} + \delta \tag{1}$$

where L_{ij} (i, j = A, B, and C) represents the self-inductance or mutual inductance of the asymmetric winding, while L_{sij} (i, j = A, B, and C) represents its symmetric component.

In PMLSM, asymmetry may occur in the self-inductance or mutual inductance of any phase winding. When different types of asymmetry occur in the machine, the specific equations of the machine change accordingly. This complicates control and estimation. Therefore, it is necessary to establish the universal model capable of describing all asymmetry cases.

To facilitate the establishment of the unified model for estimation and control, the asymmetry machine models are developed in both synchronous and stationary reference frames. The asymmetric inductance components are incorporated into the three-phase inductance matrix, then the three-phase equation is transformed into the respective reference frames. The initial

TABLE I
ASYMMETRY-RELATED PARAMETERS UNDER DIFFERENT ASYMMETRY CASES

Cases	L_i ($L_i = L_d, L_q, L_{sm}$)	γ	b_r	b_s
M_{AB}	$L_{i0} - \frac{1}{3}\delta$	$\frac{2}{3}\delta$	$-2\pi/3$	$2\pi/3$
M_{AC}			$2\pi/3$	$-2\pi/3$
M_{BC}	($L_{i0} = L_{d0}, L_{q0}, L_{sm0}$)		0	0
L_A	$L_{i0} + \frac{1}{3}\delta$	$\frac{1}{3}\delta$	0	0
L_B			$2\pi/3$	$-2\pi/3$
L_C	($L_{i0} = L_{d0}, L_{q0}, L_{sm0}$)		$-2\pi/3$	$2\pi/3$

machine equations obtained from the transformation still vary with the changes of asymmetry cases. Therefore, appropriate parameter substitutions are required to normalize all asymmetry cases. The obtained unified asymmetry machine model in the synchronous reference frame can be expressed as

$$\begin{bmatrix} u_d \\ u_q \end{bmatrix} = \begin{bmatrix} R_s - \gamma\omega_e \sin(2\theta_r + b_r) & -\omega_e L_q - \gamma\omega_e \cos(2\theta_r + b_r) \\ \omega_e L_d - \gamma\omega_e \cos(2\theta_r + b_r) & R_s + \gamma\omega_e \sin(2\theta_r + b_r) \end{bmatrix} \begin{bmatrix} i_d \\ i_q \end{bmatrix} + \begin{bmatrix} L_d + \gamma\cos(2\theta_r + b_r) & -\gamma\sin(2\theta_r + b_r) \\ -\gamma\sin(2\theta_r + b_r) & L_q - \gamma\cos(2\theta_r + b_r) \end{bmatrix} \begin{bmatrix} pi_d \\ pi_q \end{bmatrix} + \omega_e \psi_f \begin{bmatrix} 0 \\ 1 \end{bmatrix} \tag{2}$$

where u_{d}, u_{q}, and i_{d}, i_{q} are the voltages and currents in the synchronous reference frame; p is the differential operator; θ_{r} is the machine electrical angle; ω_{e} is the electrical angular velocity; R_{s} is the phase resistance; ψ_{f} is the permanent magnet flux linkage; L_{d}, L_{q}, γ, and b_{r} are associated with asymmetry, and their specific expressions will be discussed later. Similarly, the unified asymmetry model in the stationary reference frame can be obtained as

$$\begin{bmatrix} u_\alpha \\ u_\beta \end{bmatrix} = \begin{bmatrix} L_{sm} + \gamma\cos(b_s) + L_{rs}\cos 2\theta_r & \gamma\sin(b_s) + L_{rs}\sin 2\theta_r \\ \gamma\sin(b_s) + L_{rs}\sin 2\theta_r & L_{sm} - \gamma\cos(b_s) - L_{rs}\cos 2\theta_r \end{bmatrix} \begin{bmatrix} pi_\alpha \\ pi_\beta \end{bmatrix} + \begin{bmatrix} R_s - 2L_{rs}\omega_e \sin 2\theta_r & 2L_{rs}\omega_e \cos 2\theta_r \\ 2L_{rs}\omega_e \cos 2\theta_r & R_s + 2L_{rs}\omega_e \sin 2\theta_r \end{bmatrix} \begin{bmatrix} i_\alpha \\ i_\beta \end{bmatrix} + \omega_e \psi_f \begin{bmatrix} -\sin\theta_r \\ \cos\theta_r \end{bmatrix} \tag{3}$$

where u_α, u_β and i_α, i_β are the voltages and currents in the stationary reference frame, L_{rs} is the inductance parameter, and L_{sm} and b_{s} are parameters related to asymmetry.

The specific expressions of the asymmetry-related parameters are presented in Table I. γ is related to the magnitude of the asymmetry component, b_{r} and b_{s} are associated with the phase of the asymmetry component. L_{d0}, L_{q0}, and L_{sm0} represent the symmetric components of the inductance parameters, which are typically utilized for symmetric machines. Their expressions are shown in (4) and (5), where L_{s0}, L_{s2} and M_{s0}, M_{s2} represent the magnitudes of dc and ac components in symmetric self and mutual inductance. On the basis of L_{d0}, L_{q0}, and L_{sm0}, asymmetry components related to the asymmetry cases are superimposed

to obtain L_{d}, L_{q}, and L_{sm}, as shown in Table I

$$\begin{cases} L_{d0} = L_{s0} + L_{s2}/2 - M_{s0} + M_{s2} \\ L_{q0} = L_{s0} - L_{s2}/2 - M_{s0} - M_{s2} \end{cases} \tag{4}$$

$$\begin{cases} L_{sm0} = L_{s0} - M_{s0} \\ L_{rs} = L_{s2}/2 + M_{s2} \end{cases}. \tag{5}$$

The asymmetry cases in Table I indicate scenarios where the asymmetry component appears solely in the self-inductance or mutual inductance of a specific phase. When multiple asymmetry cases occur simultaneously, the model in (2) and (3) can still be applied to describe the asymmetries through linear superposition. Consequently, by accurately estimating all parameters in (2) and (3), it is feasible to compensate for model errors resulting from asymmetry, thus eliminating disturbances in estimation and control.

C. Model Reparameterization

The parameter coupling and nonlinearity caused by asymmetry make the estimation challenging to perform directly. To facilitate estimation, the asymmetry machine equations are reparameterized and transformed into the corresponding linear regression forms.

In the synchronous reference frame, the terms related to asymmetry parameters can be expanded through trigonometric transformation. Then, the excitation and the parameters can be extracted separately to obtain the linear regressions as

$$\begin{cases} y_d = u_d = \boldsymbol{m_d^T \theta_{dq}} \\ y_q = u_q = \boldsymbol{m_q^T \theta_{dq}} \end{cases}$$

$$\boldsymbol{m_d^T} = \begin{bmatrix} i_d & 0 & pi_d & -\omega_e i_q & \tau_{d1} & \tau_{d2} \end{bmatrix}$$

$$\boldsymbol{m_q^T} = \begin{bmatrix} i_q & \omega_e & \omega_e i_d & pi_q & \tau_{q1} & \tau_{q2} \end{bmatrix}$$

$$\boldsymbol{\theta_{dq}} = \begin{bmatrix} R_s & \psi_f & L_d & L_q & \gamma \cos b_r & \gamma \sin b_r \end{bmatrix}^T \tag{6}$$

where y_{d} and y_{q} are the inputs of linear regression. $\boldsymbol{m_{\mathrm{d}}}$ and $\boldsymbol{m_{\mathrm{q}}}$ are the excitation vectors, $\theta_{\mathbf{dq}}$ is the parameter vector. The expressions of τ_{d1}, τ_{d2}, τ_{q1}, and τ_{q2} are

$$\begin{cases} \tau_{d1} = -\omega_e \sin 2\theta_r i_d - \omega_e \cos 2\theta_r i_q + \cos 2\theta_r pi_d + \sin 2\theta_r pi_q \\ \tau_{d2} = -\omega_e \cos 2\theta_r i_d + \omega_e \sin 2\theta_r i_q - \sin 2\theta_r pi_d - \cos 2\theta_r pi_q \\ \tau_{q1} = -\omega_e \cos 2\theta_r i_d + \omega_e \sin 2\theta_r i_q - \sin 2\theta_r pi_d - \cos 2\theta_r pi_q \\ \tau_{q2} = \omega_e \sin 2\theta_r i_d + \omega_e \cos 2\theta_r i_q - \cos 2\theta_r pi_d + \sin 2\theta_r pi_q. \end{cases} \tag{7}$$

In the stationary reference frame, the linear regression can be obtained through the similar process. During the extraction, it is observed that the excitation term for $\gamma \cos b_{\mathrm{s}}$ and L_{sm} are linearly dependent. This relationship gives rise to the rank-deficiency issue during estimation. Therefore, the parameters with linearly dependent excitations are integrated together to obtain the linear regressions as

$$\begin{cases} y_\alpha = u_\alpha = \boldsymbol{m_\alpha^T \theta_\alpha} \\ y_\beta = u_\beta = \boldsymbol{m_\beta^T \theta_\beta} \end{cases}$$

$$\boldsymbol{m_\alpha^T} = \begin{bmatrix} i_\alpha & -\omega_e \sin\theta_r & pi_\alpha & \tau_\alpha & pi_\beta \end{bmatrix}$$

$$\boldsymbol{m_\beta^T} = \begin{bmatrix} i_\beta & \omega_e \cos\theta_r & pi_\beta & \tau_\beta & pi_\alpha \end{bmatrix}$$

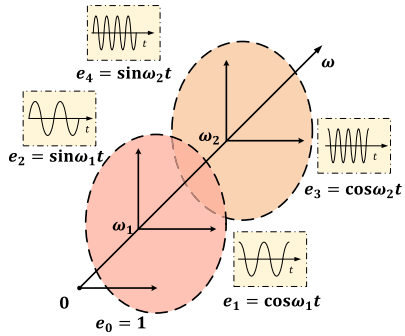

Fig. 4. Illustration of the spectrum and orthogonal basis.

$$\boldsymbol{\theta_\alpha} = \begin{bmatrix} R_s \\ \psi_f \\ L_{sm} + \gamma \cos b_s \\ L_{rs} \\ \gamma \sin b_s \end{bmatrix}, \boldsymbol{\theta_\beta} = \begin{bmatrix} R_s \\ \psi_f \\ L_{sm} - \gamma \cos b_s \\ L_{rs} \\ \gamma \sin b_s \end{bmatrix}. \tag{8}$$

In (8), y_α, y_β are the inputs, $\boldsymbol{m}_\alpha$, $\boldsymbol{m}_\beta$ and θ_α, θ_β are the excitation and parameter vectors, τ_α, τ_β are expressed as

$$\begin{cases} \tau_\alpha = -2\omega_e \sin 2\theta_r i_\alpha + 2\omega_e \cos 2\theta_r i_\beta + \cos 2\theta_r pi_\alpha + \sin 2\theta_r pi_\beta \\ \tau_\beta = 2\omega_e \cos 2\theta_r i_\alpha + 2\omega_e \sin 2\theta_r i_\beta + \sin 2\theta_r pi_\alpha - \cos 2\theta_r pi_\beta \end{cases}. \tag{9}$$

In comparison, the parameter vectors consist of two five-dimensional (5-D) vectors in the stationary reference frame, while the estimation involves one 6-D parameter vector in the synchronous reference frame. Since the computational complexity of algorithm is exponentially related to the dimension, conducting estimation with two 5-D vectors significantly reduces the computational burden. Thus, the estimation is carried out in the stationary reference frame.

III. Proposed Full Parameter Estimation Method

A. Preliminary Analysis of Estimation

Due to the increased number of estimated parameters in the PMLSM, it is necessary to conduct a preliminary analysis for the feasibility of the simultaneous full parameter estimation.

In the form of linear regression, estimation requires the excitation to satisfy the PE condition. It can be equivalently expressed in the frequency domain as requiring the reference input to contain sufficient frequency [23]. Inspired by this, the estimation conditions are analyzed from the perspective of basis in this article. The distribution of frequency in the excitation on the spectrum is illustrated in Fig. 4.

Each frequency is capable to introduce a pair of orthogonal basis vectors, represented as $\cos(\omega_{\mathrm{i}} t)$ and $\sin(\omega_{\mathrm{i}} t)$, $i \in \mathbb{N}*$. The orthogonal refers to the inner product space orthogonality, i.e., the inner product between the basis vectors is zero. A pair of orthogonal basis vectors can span a 2-D subspace. Besides, the basis vectors introduced by different frequency are linearly independent. Therefore, the n frequency can provide $2n$ basis

vectors, thereby spanning a $2n$-dimentional subspace $\mathcal{H}^{2n}$ as time varies, expressed as

$$\mathcal{H}^{2n} = \text{span}\left\{\cos\omega_1 t, \sin\omega_1 t, \ldots, \cos\omega_n t, \sin\omega_n t\right\}. \quad (10)$$

When the subspace dimension is not less than the number of estimated parameters, the input can be projected onto each orthogonal basis vector. Then, the reconstruction of the projection allows for the derivation of the parameter vector, thus achieving estimation. Therefore, the sufficiently rich excitation ensures the realization of full parameter estimation.

In PMLSM, the end effect gives rise to the detent force containing even harmonics. Consequently, the corresponding harmonic components will inevitably appear in the current during the normal operation. This state of the PMLSM is referred to as the pseudosteady state. Due to the machine operating in the pseudosteady state, its excitation term will contain enough frequency components for estimation. Therefore, despite the increased number of the estimated parameters, the presence of sufficiently rich excitation still provides the possibility of achieving full parameter estimation. It is worth noting that this is merely a preliminary analysis for feasibility, the rigorous proof will be presented below.

B. Proposed Estimation Method

To achieve full parameter estimation considering asymmetry, an enhanced estimation method is proposed in this article. The estimation method draws inspiration from the DREM method proposed in [24]. The primary objective of the estimation is to obtain the values of two parameter vectors in (8). The following illustration will focus on the α-axis as an example of the estimation algorithm. To simplify the representation, (8) is reformulated as (11), the excitations and parameters are denoted by $m_{\alpha i}$ and $\theta_{\alpha i}$, $i \in \{1, 2, \ldots, 5\}$

$$y_\alpha = u_\alpha = \boldsymbol{m}_{\boldsymbol{\alpha}}^{\boldsymbol{T}}\boldsymbol{\theta}_{\boldsymbol{\alpha}} = \begin{bmatrix} m_{\alpha1} & m_{\alpha2} & \cdots & m_{\alpha5} \end{bmatrix} \begin{bmatrix} \theta_{\alpha1} \\ \theta_{\alpha2} \\ \vdots \\ \theta_{\alpha5} \end{bmatrix}. \quad (11)$$

To extend the above linear regression equation, five stable, linear time-invariant operators $\mathcal{F}_i(\cdot)$ with $i \in \{1, 2, \ldots, 5\}$ are applied, whose transfer functions are expressed as

$$\mathcal{F}_i(s) = \frac{\alpha_i}{s + \beta_i} \quad (12)$$

where $\alpha_i, \beta_i > 0$. Another optional operator is the delay operator, which is

$$\left[\mathcal{F}_i(\cdot)\right](t) = (\cdot)(t - d_i) \quad (13)$$

where $d_i > 0$. The extended matrix equation with the operators applied can be written as

$$\boldsymbol{Y}_{\boldsymbol{\alpha}} = \boldsymbol{M}_{\boldsymbol{\alpha}}\boldsymbol{\theta}_{\boldsymbol{\alpha}}$$

$$\boldsymbol{Y}_{\boldsymbol{\alpha}} = \begin{bmatrix} y_\alpha \\ y_{\alpha f1} \\ y_{\alpha f2} \\ \cdots \\ y_{\alpha f5} \end{bmatrix}, \boldsymbol{M}_{\boldsymbol{\alpha}} = \begin{bmatrix} m_{\alpha1} & m_{\alpha2} & \cdots & m_{\alpha5} \\ m_{\alpha1f1} & m_{\alpha2f1} & \cdots & m_{\alpha5f1} \\ m_{\alpha1f2} & m_{\alpha2f2} & \cdots & m_{\alpha5f2} \\ \vdots & \vdots & \ddots & \vdots \\ m_{\alpha1f5} & m_{\alpha2f5} & \cdots & m_{\alpha5f5} \end{bmatrix} \quad (14)$$

where $y_{\alpha fi}$ and $m_{\alpha ifj}$ with $i, j \in \{1, 2, \ldots, 5\}$ are the inputs and excitations after applying operators. The extended excitation matrix is a nonsquare matrix, while subsequent processes require square regressor matrix. Hence, it needs to be transformed into a square matrix. To (14), premultiply $\boldsymbol{M}_\alpha{}^{\mathbf{H}}$ to form a square extended matrix as follows:

$$\boldsymbol{M}_{\boldsymbol{\alpha}}^{\boldsymbol{H}}\boldsymbol{Y}_{\boldsymbol{\alpha}} = \boldsymbol{M}_{\boldsymbol{\alpha}}^{\boldsymbol{H}}\boldsymbol{M}_{\boldsymbol{\alpha}}\boldsymbol{\theta}_{\boldsymbol{\alpha}}. \quad (15)$$

The matrix $\boldsymbol{M}_\alpha{}^{\mathbf{H}}$ is obtained by taking the Hermitian transpose of the $\boldsymbol{M}_\alpha$. To achieve parameter decoupling, the adjunct matrix of $\boldsymbol{M}_\alpha{}^{\mathbf{H}}\boldsymbol{M}_\alpha$ is multiplied on the left of (15), which is expressed as

$$\text{adj}\left(\boldsymbol{M}_{\boldsymbol{\alpha}}^{\boldsymbol{H}}\boldsymbol{M}_{\boldsymbol{\alpha}}\right)\boldsymbol{M}_{\boldsymbol{\alpha}}^{\boldsymbol{H}}\boldsymbol{Y}_{\boldsymbol{\alpha}} = \text{adj}\left(\boldsymbol{M}_{\boldsymbol{\alpha}}^{\boldsymbol{H}}\boldsymbol{M}_{\boldsymbol{\alpha}}\right)\boldsymbol{M}_{\boldsymbol{\alpha}}^{\boldsymbol{H}}\boldsymbol{M}_{\boldsymbol{\alpha}}\boldsymbol{\theta}_{\boldsymbol{\alpha}}. \quad (16)$$

The product of the adjunct matrix and the matrix itself yields the determinant of the matrix, thus (16) can be further expressed as

$$\boldsymbol{Y} = \phi\boldsymbol{\theta}_{\boldsymbol{\alpha}}$$

$$\boldsymbol{Y} = \text{adj}\left(\boldsymbol{M}_{\boldsymbol{\alpha}}^{\boldsymbol{H}}\boldsymbol{M}_{\boldsymbol{\alpha}}\right)\boldsymbol{M}_{\boldsymbol{\alpha}}^{\boldsymbol{T}}\boldsymbol{Y}_{\boldsymbol{\alpha}} = \begin{bmatrix} Y_1 & Y_2 & \cdots & Y_5 \end{bmatrix}^T$$

$$\phi = \begin{bmatrix} \Delta & & & \\ & \Delta & & \\ & & \ddots & \\ & & & \Delta \end{bmatrix}, \Delta = \det\left(\boldsymbol{M}_{\boldsymbol{\alpha}}^{\boldsymbol{H}}\boldsymbol{M}_{\boldsymbol{\alpha}}\right). \quad (17)$$

In this way, the vector regression equation has been transformed into separated scalar regression equations, and each parameter has a corresponding decoupled equation as

$$Y_i = \Delta\theta_{\alpha i}, i \in \bar{l} := \{1, 2, \cdots, 5\}. \quad (18)$$

Then, the gradient descent method is employed to independently estimate each parameter and expressed as

$$\dot{\hat{\theta}}_{\alpha i} = \gamma_i\Delta\left(Y_i - \Delta\hat{\theta}_{\alpha i}\right), i \in \bar{l} \quad (19)$$

where $\hat{\theta}_{\alpha i}$ represents the parameter to be estimated, and $\gamma_i > 0$ represents the adaptive gain.

Applying the same process to the linear regression in β-axis, two parameter vectors in the stationary reference frame can then be separately estimated. Based on the estimated parameter vectors $\hat{\theta}_\alpha$ and $\hat{\theta}_\beta$, the electrical parameters of the machine can be obtained through the following reconstruction:

$$\hat{R}_s, \hat{\psi}_f, \hat{L}_{sm}, \hat{L}_{rs} = \frac{\hat{\boldsymbol{\theta}}_{\boldsymbol{\alpha}}(i) + \hat{\boldsymbol{\theta}}_{\boldsymbol{\beta}}(i)}{2}, i \in \{1, 2, 3, 4\} \quad (20)$$

$$\hat{\gamma} = \sqrt{\left[\frac{\hat{\boldsymbol{\theta}}_{\boldsymbol{\alpha}}(3) - \hat{\boldsymbol{\theta}}_{\boldsymbol{\beta}}(3)}{2}\right]^2 + \left[\frac{\hat{\boldsymbol{\theta}}_{\boldsymbol{\alpha}}(5) + \hat{\boldsymbol{\theta}}_{\boldsymbol{\beta}}(5)}{2}\right]^2} \quad (21)$$

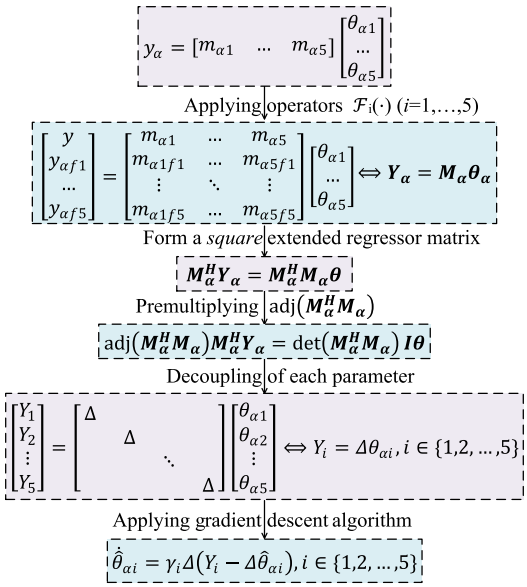

Fig. 5. Flowchart of the estimation in the α-axis.

$$\hat{b}_s = \tan^{-1}\left[\frac{\hat{\boldsymbol{\theta}}_{\boldsymbol{\alpha}}(5) + \hat{\boldsymbol{\theta}}_{\boldsymbol{\beta}}(5)}{\hat{\boldsymbol{\theta}}_{\boldsymbol{\alpha}}(3) - \hat{\boldsymbol{\theta}}_{\boldsymbol{\beta}}(3)}\right] \tag{22}$$

where $\hat{R}_s$, $\hat{L}_{sm}$, $\hat{L}_{rs}$, $\hat{\psi}_f$, $\hat{\gamma}$, and $\hat{b}_s$ are the parameters estimated by the proposed method. Based on (4) and (5), the d- and q-axis inductances can be obtained. Through the aforementioned process and algorithm, full electrical parameter estimation including asymmetry parameters can be achieved. To provide a clearer illustration, the flowchart of the linear regression estimation in the α-axis is presented in Fig. 5. The estimation in the β-axis follows the same procedure.

According to the above illustration, the proposed method has significant advantages in terms of the convergence performance. The parameter vector exhibits elementwise convergence, which is significantly stronger than the norm-based convergence observed in the conventional method. Furthermore, the estimated parameters become decoupled after the process of extension and mixing, allowing the convergence rate of each parameter to be independently tuned.

C. Stability Validation

It is essential to analyze and validate the stability of the proposed method. Based on the observability theory in [22], it can be deduced that all electrical parameters including asymmetry parameters are observable during the normal operation. However, it does not directly prove the stability of the proposed method, and the convergence performance remains unknown. Therefore, the stability analysis for the proposed method is conducted to address these concerns.

Combining the scalar regressions (18) and the gradient descent estimator (19), the estimation error $\tilde{\theta}_i = \theta_i - \hat{\theta}_i$ can be obtained as

$$\dot{\tilde{\theta}}_i = -\gamma_i \Delta^2 \tilde{\theta}_i, i \in \bar{l}. \tag{23}$$

From (23), it can be derived that the condition for the estimation error to converge to zero is equivalent to

$$\int_0^{+\infty} \Delta^2(t)\, dt = +\infty \Leftrightarrow \Delta(t) \notin \mathcal{L}_2. \tag{24}$$

When the determinant of the extended excitation matrix satisfies the condition of not belonging to the $\mathcal{L}_2$ space, each parameter can be estimated. This condition is strictly weaker than the PE condition required for the excitation term $\boldsymbol{m}^{\mathbf{T}}$ in the conventional method. It indicates that the proposed method can relax the PE condition and achieve estimation under the new stability condition. As illustrated in Section III-A, the detent force inevitably introduces harmonic components into the current loop, even under constant speed conditions. Thus, the d- and q-axis currents can be expressed as

$$\begin{cases} i_d = i_{d0} + \sum\limits_k i_{dk} \cos\left(k\omega_e t + \phi_{dk}\right) \\ i_q = i_{q0} + \sum\limits_k i_{qk} \cos\left(k\omega_e t + \phi_{qk}\right) \end{cases} \tag{25}$$

where i_{d0}, i_{q0} and i_{dk}, i_{qk} are the constant and harmonic components, ϕ_{dk}, ϕ_{qk} are the phase of the kth harmonics, $k = 2j$ ($j \in \mathbb{N}*$). To simplify the validation process, only one nth harmonic component is considered first. The impact of additional harmonic components will be illustrated later. The currents containing nth harmonic component are transformed into the stationary reference frame and simplified as

$$\begin{cases} i_\alpha = i_{d0}\cos\omega_e t - i_{q0}\sin\omega_e t + \frac{1}{2} i_{dn}\cos\left(n-1\right)\omega_e t \\ \quad + \frac{1}{2} i_{qn}\sin\left(n-1\right)\omega_e t + \frac{1}{2} i_{dn}\cos\left(n+1\right)\omega_e t \\ \quad - \frac{1}{2} i_{qn}\sin\left(n+1\right)\omega_e t \\ i_\beta = i_{d0}\sin\omega_e t + i_{q0}\cos\omega_e t + \frac{1}{2} i_{qn}\cos\left(n-1\right)\omega_e t \\ \quad - \frac{1}{2} i_{dn}\sin\left(n-1\right)\omega_e t + \frac{1}{2} i_{dn}\sin\left(n+1\right)\omega_e t \\ \quad + \frac{1}{2} i_{qn}\cos\left(n+1\right)\omega_e t \end{cases} \tag{26}$$

where i_{dn}, i_{qn} are the amplitude of the nth harmonic. The phase has been omitted here, and it will be evident in the subsequent derivation that the phase does not affect the stability condition. Taking the derivative of the currents yields the expressions for pi_α and pi_β. Then, substitute them into the excitation vector to obtain its specific expression. The following derivation takes the α-axis excitation as an example. By extracting the frequency components as orthogonal basis vectors, the excitation vector $\boldsymbol{m}_\alpha$ can be decomposed into the product of the coefficient matrix $\boldsymbol{X}^{\mathbf{T}}$ and the basis vector $\boldsymbol{\xi}$, as illustrated in (27) shown at the bottom of next page.

When applying five linear operators $\mathcal{F}_i(\cdot)$ with $i \in \{1, 2, \ldots, 5\}$ to the excitation vector, the extended excitation matrix $\boldsymbol{M}_\alpha$ can be expressed as (28) shown at the bottom of next page. In (28), $(n\text{-}1)\omega_{\mathrm{e}}$ and $(n{+}1)\omega_{\mathrm{e}}$ are expressed as ω_{e1} and ω_{e2}. The effect of the adopted linear operators can be characterized by amplitude variations and phase shifts of the frequency components within the basis vector $\boldsymbol{\xi}$, which are represented by A_{ij} and d_{ij}, $i \in \{1, 2, 3\}$, $j \in \{1, 2, \ldots, 5\}$. Extract the frequency components from the extended excitation and place them in the diagonal matrix $\boldsymbol{D}$. Then, the effect of the linear operators on each frequency component can be represented by the impact matrix $\boldsymbol{E}$. In this

way, $\boldsymbol{M}_\alpha$ can be decomposed into three matrices, as shown in

$$\boldsymbol{M_\alpha} = \boldsymbol{E}_{6\times6}\boldsymbol{D}_{6\times6}\boldsymbol{X}_{6\times5}. \tag{29}$$

Since, it is necessary to determine whether the determinant of ${\boldsymbol{M}_\alpha}^{\mathbf{H}}\boldsymbol{M}_\alpha$ satisfies the nonsquare integrability condition, the rank of $\boldsymbol{M}_\alpha$ is analyzed first. For the impact matrix $\boldsymbol{E}$, it is straightforward to achieve full rank by setting different coefficients of five linear operators. For the diagonal matrix $\boldsymbol{D}$, as long as the frequency components are sufficiently rich and the machine speed is not zero, this matrix has full rank. For the third matrix $\boldsymbol{X}$, by calculating the determinant of $\boldsymbol{X}^{\mathbf{T}}\boldsymbol{X}$, the sufficient condition for $\boldsymbol{X}$ to have full column rank can be derived, which is presented as (30). As the pseudosteady state of the PMLSM will inevitably introduce ripples into the currents, this condition can be satisfied

$$i_{dn} \neq 0 \,\&\&\, i_{q0}i_{qn} \neq 0 \,\&\&\, \omega_e \neq 0 \Rightarrow \text{rank}\left(\boldsymbol{X}_{6\times5}\right) = 5. \tag{30}$$

Based on the Sylvester's rank inequality, (31) can be obtained, n_0 represents the column number of $\boldsymbol{D}$, which is 6

$$\text{rank}\left(\boldsymbol{D}_{6\times6}\boldsymbol{X}_{6\times5}\right) \geq \text{rank}\left(\boldsymbol{D}_{6\times6}\right) + \text{rank}\left(\boldsymbol{X}_{6\times5}\right) - n_0. \tag{31}$$

By substituting the rank of $\boldsymbol{D}$, it can be derived that the rank of $\boldsymbol{DX}$ is not less the rank of $\boldsymbol{X}$. In addition, the rank of $\boldsymbol{DX}$ is not greater than the rank of $\boldsymbol{X}$. Thus, the ranks of the two are equal. Through the same process, it is obtained that $\boldsymbol{M}_\alpha$ has full column rank. Since the rank of a matrix remains unchanged after multiplying it by its Hermitian transpose, ${\boldsymbol{M}_\alpha}^{\mathbf{H}}\boldsymbol{M}_\alpha$ has full rank, as shown in

$$\text{rank}\left(\boldsymbol{M}_{\boldsymbol{\alpha}}^{\boldsymbol{H}}\boldsymbol{M}_{\boldsymbol{\alpha}}\right) = \text{rank}\left(\boldsymbol{M}_{\boldsymbol{\alpha}}\right) = \text{rank}\left(\boldsymbol{X}_{6\times5}\right) = 5. \tag{32}$$

Since ${\boldsymbol{M}_\alpha}^{\mathbf{H}}\boldsymbol{M}_\alpha$ has full rank, it can be inferred that its determinant is not zero. For the matrices that compose $\boldsymbol{M}_\alpha$, it is observed that $\boldsymbol{E}$ and $\boldsymbol{X}$ are constant matrices, while $\boldsymbol{D}$ is the matrix composed of trigonometric functions. Consequently, the determinant must be formed by the linear superposition of a series of trigonometric functions as (33) with $\lambda := \{1, n_1, n_2\}$

$$\Delta = \det\left(\boldsymbol{M}_{\boldsymbol{\alpha}}^{\boldsymbol{H}}\boldsymbol{M}_{\boldsymbol{\alpha}}\right) = \sum_{k\in\lambda} A_k\text{cos}k\omega_e t + B_k\text{sin}k\omega_e t \tag{33}$$

where A_k and B_k are the coefficients of each frequency component obtained after the aforementioned extension and mixing process. Squaring the above determinant and decomposing it based on the product-to-sum identities yields the following equation with $\lambda_0 := \{n_1 \pm 1, n_2 \pm 1, n_1 \pm n_2\}$:

$$\Delta^2 = \sum_{i\in\lambda} \frac{A_i^2 + B_i^2}{2} + \sum_{k\in\lambda_0} A_k\text{cos}k\omega_e t + B_k\text{sin}k\omega_e t. \tag{34}$$

According to (24), the stability condition can be satisfied if and only if Δ is nonintegrable. In (34), Δ^2 contains constant terms and time-varying terms composed of multiple frequency components. As illustrated in (35) and (36) below, the integral results for the constant terms are infinite, and the integral results for the time-varying terms have upper and lower bounds. Thus, the sum of the two remains infinite, indicating that Δ possesses

$$\boldsymbol{m_\alpha} = \frac{1}{2}\begin{bmatrix} 2i_{d0} & -2i_{q0} & i_{dn} & i_{qn} & i_{dn} & -i_{qn} \\ -2\omega_e i_{q0} & -2\omega_e i_{d0} & (n-1)\,\omega_e i_{qn} & -(n-1)\,\omega_e i_{dn} & -(n+1)\,\omega_e i_{qn} & -(n+1)\,\omega_e i_{dn} \\ 2\omega_e i_{q0} & -2\omega_e i_{d0} & -(n-1)\,\omega_e i_{qn} & -(n-1)\,\omega_e i_{dn} & (n+1)\,\omega_e i_{qn} & -(n+1)\,\omega_e i_{dn} \\ 0 & -2\omega_e & 0 & 0 & 0 & 0 \\ 2\omega_e i_{d0} & -2\omega_e i_{q0} & -(n-1)\,\omega_e i_{dn} & -(n-1)\,\omega_e i_{qn} & (n+1)\,\omega_e i_{dn} & -(n+1)\,\omega_e i_{qn} \end{bmatrix}\begin{bmatrix} \text{cos}\omega_e t \\ \text{sin}\omega_e t \\ \text{cos}\,(n-1)\,\omega_e t \\ \text{sin}\,(n-1)\,\omega_e t \\ \text{cos}\,(n+1)\,\omega_e t \\ \text{sin}\,(n+1)\,\omega_e t \end{bmatrix} = \boldsymbol{X^T\xi} \tag{27}$$

$$\boldsymbol{M_\alpha} = \mathcal{F}\left(\boldsymbol{m_\alpha^T}\right) = \begin{bmatrix} \boldsymbol{m_\alpha^T} \\ \mathcal{F}_1\left(\boldsymbol{m_\alpha^T}\right) \\ \vdots \\ \mathcal{F}_5\left(\boldsymbol{m_\alpha^T}\right) \end{bmatrix} = \begin{bmatrix} \boldsymbol{\xi^T} \\ \mathcal{F}_1\left(\boldsymbol{\xi^T}\right) \\ \vdots \\ \mathcal{F}_5\left(\boldsymbol{\xi^T}\right) \end{bmatrix}\boldsymbol{X}$$

$$= \begin{bmatrix} \text{cos}\omega_e t & \text{sin}\omega_e t & \text{cos}(\omega_{e1}t) & \text{sin}(\omega_{e1}t) & \text{cos}(\omega_{e2}t) & \text{sin}(\omega_{e2}t) \\ A_{11}\,\text{cos}(\omega_e t - d_{11}) & A_{11}\text{sin}(\omega_e t - d_{11}) & A_{21}\,\text{cos}(\omega_{e1}t - d_{21}) & A_{21}\,\text{sin}(\omega_{e1}t - d_{21}) & A_{31}\,\text{cos}(\omega_{e2}t - d_{31}) & A_{31}\,\text{sin}(\omega_{e2}t - d_{31}) \\ \vdots & \vdots & \vdots & \vdots & \vdots & \vdots \\ A_{15}\,\text{cos}(\omega_e t - d_{15}) & A_{15}\text{sin}(\omega_e t - d_{15}) & A_{25}\,\text{cos}(\omega_{e1}t - d_{25}) & A_{25}\,\text{sin}(\omega_{e1}t - d_{25}) & A_{35}\,\text{cos}(\omega_{e2}t - d_{35}) & A_{35}\,\text{sin}(\omega_{e2}t - d_{35}) \end{bmatrix}\boldsymbol{X}$$

$$= \begin{bmatrix} 1 & 1 & \dots & 1 & 1 \\ A_{11}\,(\text{cos}d_{11} - \text{sin}d_{11}) & A_{11}\,(\text{cos}d_{11} + \text{sin}d_{11}) & \dots & A_{31}\,(\text{cos}d_{31} - \text{sin}d_{31}) & A_{31}\,(\text{cos}d_{31} + \text{sin}d_{31}) \\ \vdots & \vdots & \ddots & \vdots & \vdots \\ A_{15}\,(\text{cos}d_{15} - \text{sin}d_{15}) & A_{15}\,(\text{cos}d_{15} + \text{sin}d_{15}) & \dots & A_{35}\,(\text{cos}d_{35} - \text{sin}d_{35}) & A_{35}\,(\text{cos}d_{n25} + \text{sin}d_{35}) \end{bmatrix}\boldsymbol{DX}$$

$$\boldsymbol{D} = \text{diag}\left(\text{cos}\omega_e t, \text{sin}\omega_e t, \text{cos}\left(n_1\omega_e t\right), \text{sin}\left(n_1\omega_e t\right), \text{cos}\left(n_2\omega_e t\right), \text{sin}\left(n_2\omega_e t\right)\right) \tag{28}$$

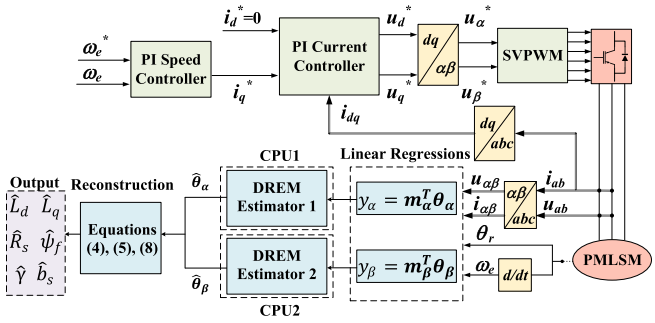

Fig. 6. Block diagram of the entire control and estimation system.

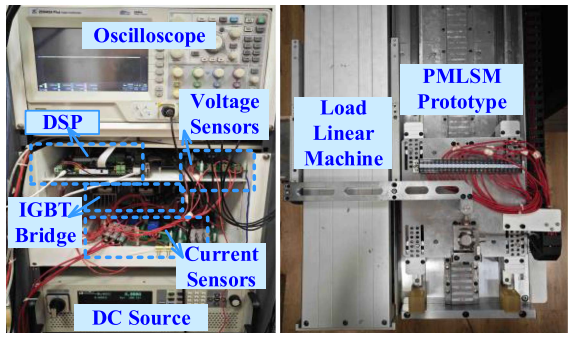

Fig. 7. Experiment platform.

characteristic of nonsquare integrability

$$\int_0^\infty \left(\sum_{i\in\lambda} \frac{A_i^2 + B_i^2}{2} \right) dt = +\infty \tag{35}$$

$$\sup \left| \int_0^\infty \left(\sum_{k\in\lambda_0} A_k \cos k\omega_e t + B_k \sin k\omega_e t \right) dt \right| = \sum_{k\in\lambda_0} |A_k| + |B_k| \,. \tag{36}$$

When there are more frequency components in the excitation, as they are linearly independent, it does not affect the conclusion about rank and nonsquare integrability. Hence, the stability condition can still be satisfied. The proof for the estimation condition in the β-axis can be similarly demonstrated. Therefore, utilizing the proposed method, estimation can be achieved separately in the α-/β-axis, ultimately leading to the full parameter estimation.

IV. Experimental Validation

The feasibility and effectiveness of the proposed method have been validated through experiments. The estimation method is integrated into the control system, and the block diagram of the entire machine control system is shown in Fig. 6. To mitigate the impact of inverter nonlinearity, the voltage sensors are employed for voltage measurement.

A. Experimental Platform and Setup

The experiment platform with the PMLSM prototype, load linear machine, and the control system is depicted in Fig. 7. The oscilloscope is utilized to store and export the experimental data. The sampling and control periods are both set to 100 μs. The controller processor is TMS320F28379D DSP. It incorporates two CPUs with the ability to execute parallel computations and communicate with each other. Meanwhile, the estimation processes of the α-/β-axis linear regressions in the proposed method are independent. Therefore, the estimation algorithm will be executed in parallel on two CPUs to ensure a 10 kHz update rate.

The offline measurement methods summarized in [21] are employed to obtain the electromagnetic parameters of the PMLSM prototype. Fig. 8 shows the measured inductance results. There

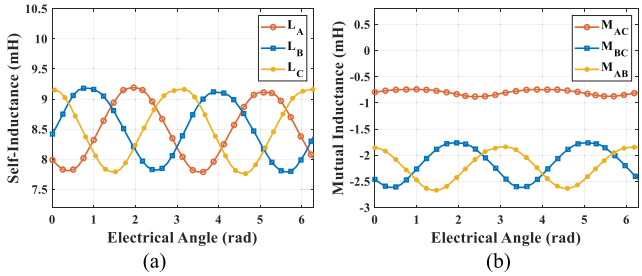

Fig. 8. Measured inductance. (a) Self-inductance. (b) Mutual inductance.

TABLE II
Parameters of PMLSM Prototype

Parameters	Value
Stator Resistance (Ω), R_s	0.7
PM Flux Linkage (Wb), ψ_f	0.05
d-axis Symmetric Inductance (mH), L_{d0}	10
q-axis Symmetric Inductance (mH), L_{q0}	11.6
Asymmetric Component (mH), δ	1.45
Asymmetric Phase Parameter (°), b_s	-120
Pitch length (mm)	15

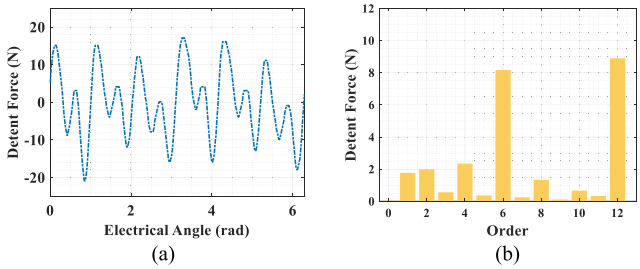

Fig. 9. Measured detent force. (a) Detent force. (b) Spectrum.

is asymmetric component in the ac mutual inductance, which is consistent with the FE simulation results. And all measured parameters are summarized in Table II.

The measurement result of the detent force is shown in Fig. 9. The detent force exhibits multiple even-order harmonic components, as illustrated in its spectrum. Thus, the preconditions for parameter estimation can be satisfied.

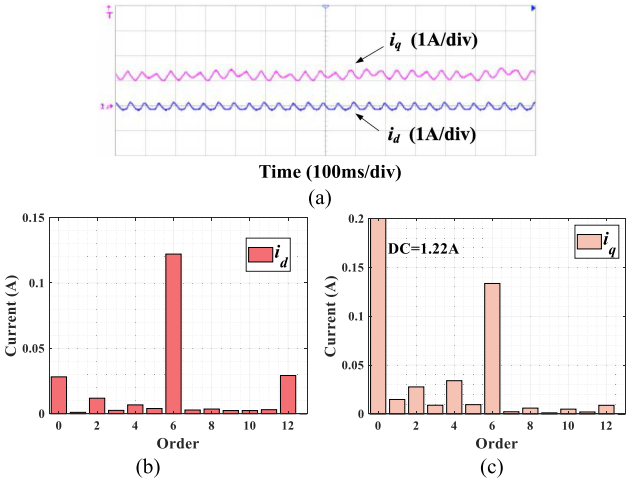

Fig. 10. Measured currents at no-load with velocity 0.1 m/s. (a) Currents. (b) Spectrum of d-axis current. (c) Spectrum of q-axis current.

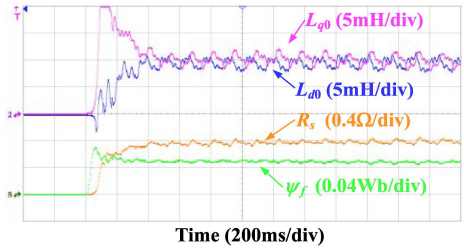

Fig. 11. Estimation results of conventional two RLS methods.

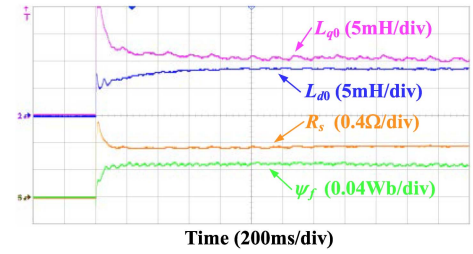

Fig. 12. Estimation results of EKF method.

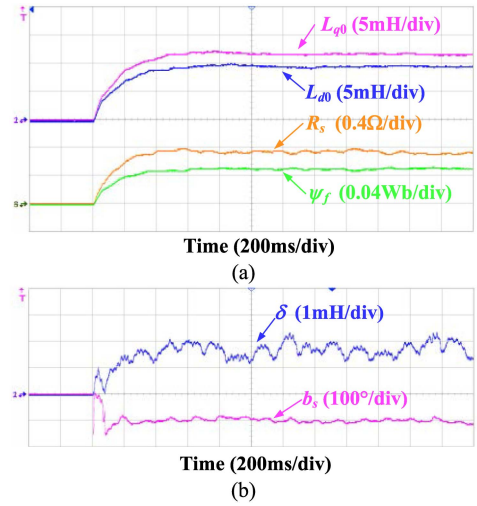

Fig. 13. Results of the proposed method. (a) L_{d0}, L_{q0}, R_{s}, and ψ_{f}. (b) δ and b_{s}.

When the speed of PMLSM is controlled at no-load with velocity 0.1 m/s, the currents are shown in Fig. 10. Owing to the presence of detent force, even-order harmonics are coupled into the currents. Moreover, the frequency in the currents is more diverse than the frequency employed in the proof above. Consequently, the stability conditions become easier to satisfy.

B. Comparative Validation

To verify the feasibility of the proposed estimation method and demonstrate its superiority in terms of convergence performance, the comparative study with existing estimation methods is conducted. The first conventional estimation method employed for comparison is proposed in [20]. The parameters are estimated with RLS utilizing different time scales, namely the high sampling rate for inductances and the low sampling rate for resistance and flux linkage. The second estimation method replaces the RLS with the EKF, which exhibits superior robustness against disturbances including model uncertainties and measurement noise [29]. In the proposed method, the delay operators with the delay times of $(0.02k)$s ($k\in\{12,34,5\}$) are utilized as linear operators. Under the conditions of the speed of 0.1 m/s at no load, the estimation results of three methods are depicted in Figs. 11 –13.

First, the steady-state estimation performance of three methods is compared. In Fig. 11, when employing the RLS method, the model errors resulting from the neglected asymmetric parameters are coupled into the results of all parameters, particularly in the inductances. In Fig. 12, the estimation results obtained through the EKF demonstrate improved stability, while slight fluctuations caused by asymmetry persist in the q-axis inductance. Fig. 13 illustrates that when the proposed estimation method is applied, all six electrical parameters, including asymmetry parameters, can be reliably and stably estimated. Due to the consideration of asymmetry, the ripples in the inductances have significantly decreased. The specific estimation results are presented in Table III. It is observed that significant errors still exist in the results of EKF, indicating that the disturbance caused by asymmetry cannot be entirely eliminated. Compared to the two methods without considering asymmetry, the proposed method exhibits higher estimation accuracy and enhanced stability. Furthermore, only through the proposed method can the asymmetry parameters be estimated.

To facilitate a more intuitive comparison of the dynamic estimation performance of the three methods, the estimation results of parameters are presented on the same figure, as depicted in Fig. 14.

In Fig. 14, the three estimation methods demonstrate comparable convergence rates. In the estimation results of the RLS and EKF methods, certain parameters exhibit noticeable overshoots during the convergence process. It is because the parameters

TABLE III
ESTIMATION RESULTS OF CONVENTIONAL AND PROPOSED METHODS

Parameters	RLS			EKF			Proposed Method		
	Average	Error (%)	Ripple (%)	Average	Error (%)	Ripple (%)	Average	Error (%)	Ripple (%)
L_{d0} (mH)	9.44	5.6	16.9	8.73	12.7	2.3	9.52	4.8	4.2
L_{q0} (mH)	10.41	10.3	18.3	10.75	7.3	4.7	12.03	-3.7	3.4
R_s (Ω)	0.77	-10.0	7.3	0.75	-7.1	2.1	0.73	-4.3	5.7
ψ_f (Wb)	0.047	6.0	6.7	0.048	4.0	4.8	0.049	2.0	4.9
δ (mH)	-	-	-	-	-	-	1.62	11.7	34.7
b_s (°)	-	-	-	-	-	-	-104	13.3	17.6

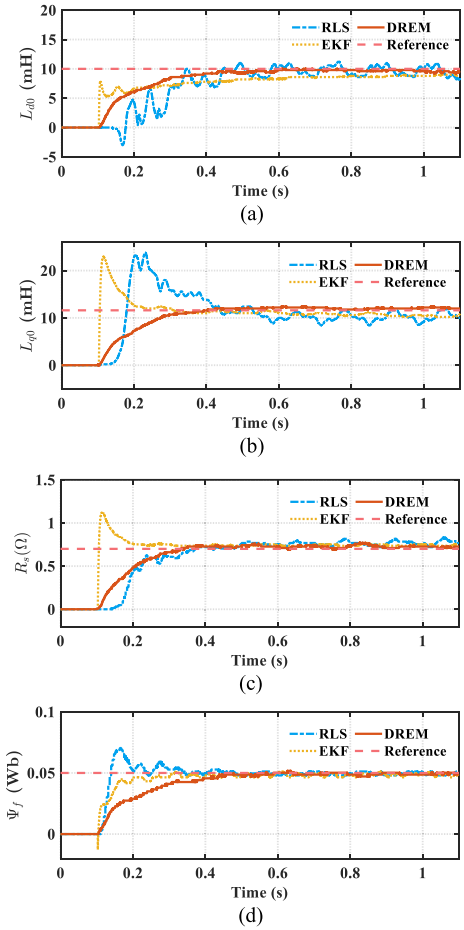

Fig. 14. Estimation results of the three methods. (a) L_{d0}. (b) L_{q0}. (c) R_s. (d) ψ_f.

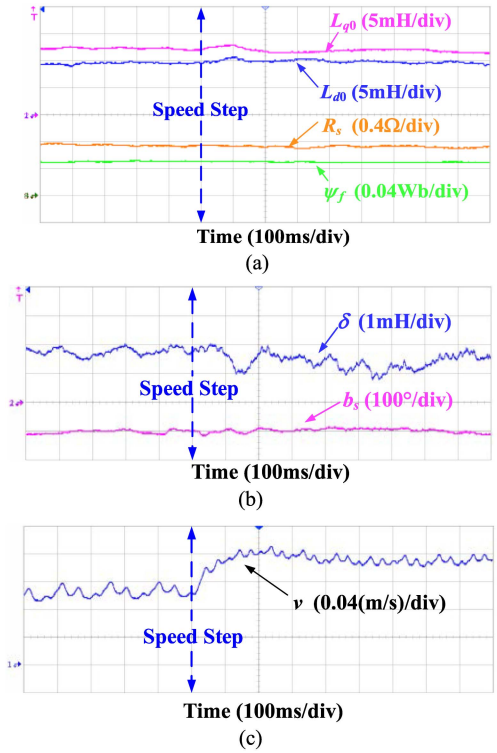

Fig. 15. Estimation results of proposed method in the speed step. (a) L_{d0}, L_{q0}, R_s, and ψ_f. (b) δ and b_s. (c) Speed.

converge based on the norm of parameter vector, which leads to inconsistent convergence processes for each parameter. To the proposed method, the estimated parameters converge element-wise, and the entire convergence process is much more stable without pronounced overshoot.

C. Robustness Validation

To further demonstrate the robustness of the proposed method, the estimation performance is verified under different disturbance scenarios. In this article, the speed step and load disturbance experiments are conducted. In the speed step experiment, when the given speed is increased from 0.1 to 0.15 m/s at no load, the estimation results of the proposed method are shown in Fig. 15. In the load disturbance experiment, the load is increased from 50 to 80 N while the speed is set at 0.1 m/s. The results under the changed load conditions are depicted in Fig. 16.

In the speed step experiment, certain ripples exist in the estimation results when the speed undergoes a sudden change. However, these parameters can quickly stabilize and return to their normal values. Moreover, the change in speed does not impact the estimation accuracy. As illustrated in Fig. 16, there are fluctuations in the estimated parameters when the load suddenly increases. On the other hand, the overall stability of the estimation results can still be guaranteed. Therefore, it can be demonstrated that the proposed method exhibits strong

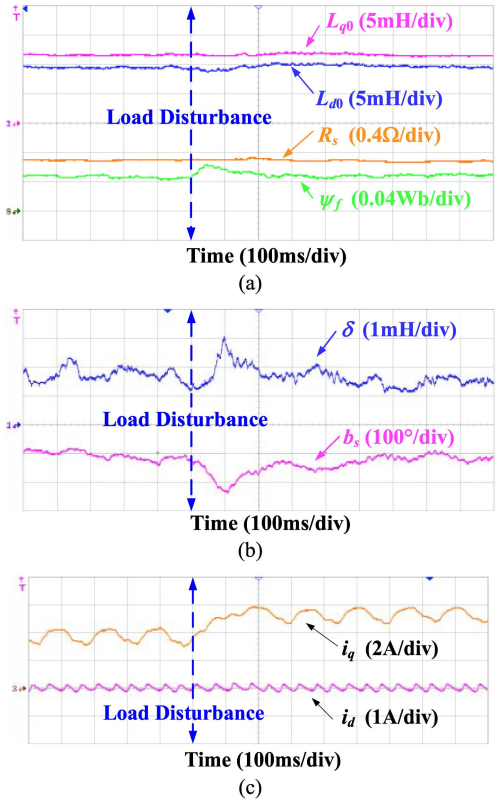

Fig. 16. Estimation results of the proposed method in the load disturbance. (a) L_{d0}, L_{q0}, R_{s}, and ψ_{f}. (b) δ and b_{s}. (c) Currents.

robustness and stability under different working conditions and disturbances.

D. Control Applications

To underscore the significance of the proposed estimation method in the context of control system, the experiments are conducted by integrating the estimation into control methods. In the experiments, the control methodology employed is the deadbeat predictive current control (DPCC). It is characterized by its high precision and rapid response, and its performance is highly dependent on the model accuracy [30].

The comparative experiments are carried out to assess the control performance before and after the implementation of the proposed estimation method. The current harmonics induced by detent force make comparison unclear. Thus, the current tracking errors are extracted and presented. Before initiating estimation, the DPCC utilizes nominal parameters without considering asymmetry. After enabling the estimation, all estimated electrical parameters are employed in DPCC. At no-load with velocity 0.1 m/s, the current tracking errors are illustrated in Fig. 17. To compare and validate the impact of different operating conditions, the experiments are conducted by varying the speed to 0.06 m/s and increasing the load to 50 N. The results are depicted in Figs. 18 and 19, respectively.

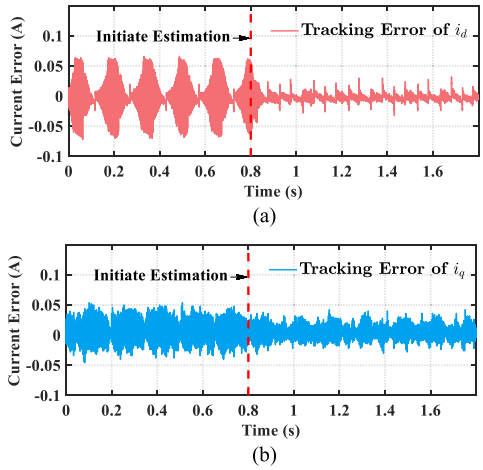

Fig. 17. Measured current tracking errors at no-load with velocity 0.1 m/s. (a) i_{d}. (b) i_{q}.

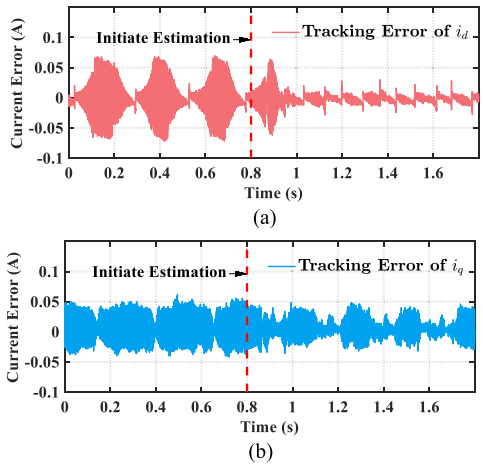

Fig. 18. Measured current tracking errors at no-load with velocity 0.06 m/s. (a) i_{d}. (b) i_{q}.

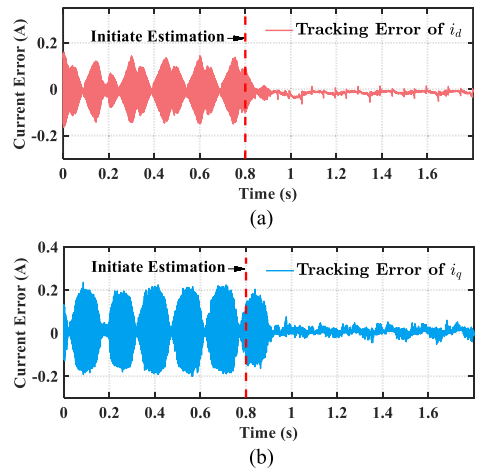

Fig. 19. Measured current tracking errors at load of 50 N with velocity 0.1 m/s. (a) i_{d}. (b) i_{q}.

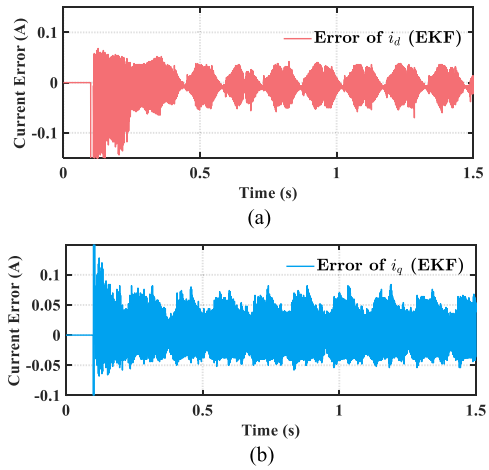

Fig. 20. Measured current tracking errors with EKF. (a) d-axis current. (b) q-axis current.

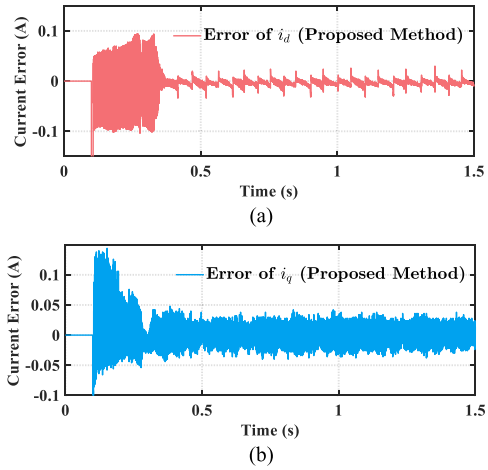

Fig. 21. Measured current tracking errors with the proposed method. (a) d-axis current. (b) q-axis current.

As illustrated in Figs. 17–19, under different speed and load conditions, the current tracking errors exhibit pronounced second harmonic components before initiating the estimation. This is attributed to the neglect of asymmetry parameters. As the load increases, the amplitude of harmonic components also increases. After initiating the estimation method, the second harmonic errors under various operating conditions are significantly diminished following a brief period of convergence. This indicates that accurate estimation and application of asymmetry parameters can effectively mitigate the tracking errors caused by asymmetry. Furthermore, it demonstrates the crucial importance and effectiveness of the proposed estimation method in enhancing control accuracy.

To compare the differences in control performance when employing the estimation methods without and with considering asymmetry, both the EKF and the proposed estimation method are activated at the beginning of control. The current tracking errors at no-load with velocity 0.1 m/s are then compared. To validate the robustness against parameter mismatch, the initial parameters are modified to twice their nominal values, and the asymmetry parameters are set to zero. The results are illustrated in Figs. 20 and 21.

Based on the experimental results of both methods, it can be observed that as the estimated parameters converge, the current tracking errors decrease. It means that both methods possess the capability to mitigate the impact of parameter mismatch. However, due to the absence of consideration and estimation for asymmetry parameters when adopting EKF method, the tracking errors still exhibit noticeable second harmonic components. In contrast, the results of the proposed method display significantly smaller tracking errors, especially in terms of the second harmonic components. Therefore, compared to the conventional estimation methods without considering asymmetry, the proposed estimation method provides notable advantages in improving control performance through additional estimation of asymmetry parameters.

V. Conclusion

An enhanced method for full electrical parameter estimation considering asymmetry is proposed. The stability condition is demonstrated from the perspectives of basis, thereby new insights for stability analysis is provided. The feasibility and advantages of the proposed method are further verified through experiments. The conclusions are drawn as follows.

1) The proposed method possesses full parameter estimation capability without adding any external excitation. It significantly reduces the estimation ripples to obtain precise steady-state performance, with the estimation errors of the fundamental parameters within 5% and the error of asymmetric parameter merely 11% despite its inherently small value. It exhibits similar accuracy to the asymmetric HFI method, while avoiding any impact on the machine operation.
2) The proposed method exhibits enhanced dynamic estimation performance. During the estimation process, each parameter converges elementwise with the stable convergence process even under different disturbance scenarios, such as speed steps and load disturbances.
3) By applying the proposed estimation method to the control strategy, enhanced control performance can be achieved. Compared to the conventional estimation method, the proposed method can effectively eliminate disturbances caused by asymmetry through additional estimation of asymmetry parameters, thereby improving control accuracy and stability.

References

[1] F. Wang, L. He, J. Kang, R. Kennel, and J. Rodríguez, "Adaptive model predictive current control for PMLSM drive system," *IEEE Trans. Ind. Electron.*, vol. 70, no. 4, pp. 3493–3502, Apr. 2023.

[2] Z. Xie, Q. Lu, W. Mei, and Y. Li, "Improved analytical modeling of a novel ironless linear synchronous machine with asymmetrical double-layer winding topology," *IEEE Trans. Ind. Appl.*, vol. 57, no. 2, pp. 1411–1419, Mar./Apr. 2021.

[3] Y. Zhang, X. Huang, A. Wang, and J. Xu, "A position and speed controller tuning method of permanent magnet synchronous linear motor based on gain identification," *IEEE Trans. Power. Electron.*, vol. 37, no. 10, pp. 11716–11724, Oct. 2022.
[4] Q. Lu, B. Wu, Y. Yao, Y. Shen, and Q. Jiang, "Analytical model of permanent magnet linear synchronous machines considering end effect and slotting effect," *IEEE Trans. Energy Convers.*, vol. 35, no. 1, pp. 139–148, Mar. 2020.
[5] B. H. B. Boff, P. R. Eckert, and Y. Amara, "A comprehensive review on the end effects of linear permanent magnet machines," *IEEE Trans. Ind. Appl.*, vol. 59, no. 2, pp. 1728–1741, Mar./Apr. 2023.
[6] Z. Chen, W. Kong, C. Shi, R. Qu, and V. Fedida, "A novel negative-sequence current injection method for reducing LVPMM electromagnetic thrust ripple considering static longitudinal end effect," *IEEE Trans. Ind. Electron.*, vol. 68, no. 2, pp. 1108–1117, Feb. 2021.
[7] Z. Chen, W. Kong, R. Qu, D. Li, and C. Shi, "Symmetrical components observer for LPMM back EMF based on negative-sequence current injection," *IEEE Trans. Ind. Electron.*, vol. 69, no. 2, pp. 1346–1355, Feb. 2022.
[8] M. Zheng, Z. Zou, Q. Lu, Y. Li, and Y. Shen, "A simple modified deadbeat direct thrust control for permanent magnet linear synchronous machine considering parameter asymmetry," *IEEE Trans. Ind. Appl.*, vol. 59, no. 3, pp. 3163–3174, May/Jun. 2023.
[9] K. Huang, J. Liang, Z. Qian, and J. Li, "An iterative estimation algorithm of prepositioning focusing on the detent force in the permanent magnet linear synchronous motor system," *IEEE Trans. Ind. Electron.*, vol. 67, no. 10, pp. 8252–8261, Oct. 2020.
[10] M. S. Rafaq and J.-W. Jung, "A comprehensive review of state-of-the-art parameter estimation techniques for permanent magnet synchronous motors in wide speed range," *IEEE Trans. Ind. Inform.*, vol. 16, no. 7, pp. 4747–4758, Jul. 2020.
[11] C. Lian, F. Xiao, J. Liu, and S. Gao, "Parameter and VSI nonlinearity hybrid estimation for PMSM drives based on recursive least square," *IEEE Trans. Transport. Electrific.*, vol. 9, no. 2, pp. 2195–2206, Jun. 2023.
[12] Z. Liu, B. Shen, W. Kong, X. Fan, K. Peng, and R. Qu, "Analytical approach for position observation error correction in IPMSM sensorless drives using online multi-parameter estimation," *IEEE Trans. Power Electron.*, vol. 39, no. 8, pp. 9230–9243, Aug. 2024.
[13] S. Liu et al., "Virtual-axis injection based online parameter identification of PMSM considering cross coupling and saturation effects," *IEEE Trans. Power Electron.*, vol. 38, no. 5, pp. 5791–5802, May 2023.
[14] Z. Wang, J. Chai, X. Xiang, X. Sun, and H. Lu, "A novel online parameter identification algorithm designed for deadbeat current control of the permanent-magnet synchronous motor," *IEEE Trans. Ind. Appl.*, vol. 58, no. 2, pp. 2029–2041, Mar./Apr. 2022.
[15] Z. Q. Zhu, D. Liang, and K. Liu, "Online parameter estimation for permanent magnet synchronous machines: An overview," *IEEE Access*, vol. 9, pp. 59059–59084, 2021.
[16] Q. Wang, G. Wang, N. Zhao, G. Zhang, Q. Cui, and D. Xu, "An impedance model-based multiparameter identification method of PMSM for both offline and online conditions," *IEEE Trans. Power Electron.*, vol. 36, no. 1, pp. 727–738, Jan. 2021.
[17] P. Wang, Z. Q. Zhu, and D. Liang, "Improved position-offset based online parameter estimation of PMSMs under constant and variable speed operations," *IEEE Trans. Energy Convers.*, vol. 39, no. 2, pp. 1325–1340, Jun. 2024.
[18] K. Yu and Z. Wang, "Online decoupled multi-parameter identification of dual three-phase IPMSM under position-offset and HF signal injection," *IEEE Trans. Ind. Electron.*, vol. 71, no. 4, pp. 3429–3440, Apr. 2024.
[19] Y. Yu, X. Huang, and Z. Li, "Overall electrical parameters identification for IPMSMs using current derivative to avoid rank deficiency," *IEEE Trans. Ind. Electron.*, vol. 70, no. 7, pp. 7515–7520, Jul. 2023.
[20] S. J. Underwood and I. Husain, "Online parameter estimation and adaptive control of permanent-magnet synchronous machines," *IEEE Trans. Ind. Electron.*, vol. 57, no. 7, pp. 2435–2443, Jul. 2010.
[21] Z. Zou, M. Zheng, Y. Li, and Q. Lu, "A novel full electrical parameters estimation method of permanent magnet linear synchronous machines considering parameter asymmetry," *IEEE Trans. Ind. Electron.*, vol. 71, no. 9, pp. 10256–10267, Sep. 2024.
[22] X. Wang et al., "Optimization-based parameter estimation for PMSMs under unified observable conditions," *IEEE Trans. Power Electron.*, vol. 39, no. 2, pp. 2632–2643, Feb. 2024.
[23] S. Sastry and M. Bodson, *Adaptive Control: Stability, Convergence, and Robustness*. Englewood Cliffs, NJ, USA: Prentice-Hall, 1989.
[24] S. Aranovskiy, A. Bobtsov, R. Ortega, and A. Pyrkin, "Performance enhancement of parameter estimators via dynamic regressor extension and mixing," *IEEE Trans. Autom. Control*, vol. 62, no. 7, pp. 3546–3550, Jul. 2017.
[25] B. Yi and R. Ortega, "Conditions for convergence of dynamic regressor extension and mixing parameter estimators using LTI filters," *IEEE Trans. Autom. Control*, vol. 68, no. 2, pp. 1253–1258, Feb. 2023.
[26] J. Schiffer, P. Aristidou, and R. Ortega, "Online estimation of power system inertia using dynamic regressor extension and mixing," *IEEE Trans. Power Syst.*, vol. 34, no. 6, pp. 4993–5001, Nov. 2019.
[27] M. A. Arteaga, "On the exact parameter estimation for robot manipulators without persistence of excitation," *IEEE Trans. Autom. Control*, vol. 69, no. 1, pp. 410–417, Jan. 2024.
[28] Z. Zou, Q. Lu, Y. Li, and Z. Q. Zhu, "Dynamic regressor extension and mixing-based parameter estimation for permanent magnet linear synchronous machines considering parameter asymmetry," in *Proc. IEEE Int. Electric Mach. Drives Conf.*, 2023, pp. 1–6.
[29] X. Li and R. Kennel, "General formulation of kalman-filter-based online parameter identification methods for VSI-fed PMSM," *IEEE Trans. Ind. Electron.*, vol. 68, no. 4, pp. 2856–2864, Apr. 2021.
[30] X. Zhang, B. Hou, and Y. Mei, "Deadbeat predictive current control of permanent-magnet synchronous motors with stator current and disturbance observer," *IEEE Trans. Power Electron.*, vol. 32, no. 5, pp. 3818–3834, May 2017.

Ziyu Zou (Student Member) was born in Zhejiang, China, in 1999. He received the B.Eng. degree in electrical engineering in 2021 from Zhejiang University, Hangzhou, China, where he is currently working toward the Ph.D. degree in electrical engineering.

His research interests include the motor drive and control of permanent magnet linear machines.

Mengfei Zheng (Student Member) was born in Fuzhou, China, in 1994. He received the B.Eng. and M.Sc. degrees from Fuzhou University, Fuzhou, China, in 2016 and 2019, respectively. He is currently working toward the Ph.D. degree with the College of Electrical Engineering, Zhejiang University, Hangzhou, China, all in electrical engineering.

His research interests include analysis and control of permanent magnet linear machines, planar machines.

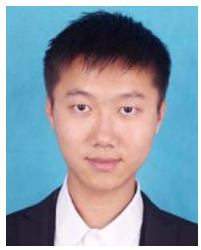

Yanxin Li (Member, IEEE) received the B.Eng. and M.Eng. degrees from Zhejiang University, Hangzhou, China, in 2011 and 2014, respectively, and the Ph.D. degree from the University of Sheffield, Sheffield, U.K., in 2018, all in electrical engineering.

Since 2020, he has been a tenure-tracked Associate Professor with the Zhejiang University. His major research interests include the modeling, design, and analysis of linear machines.

Qinfen Lu (Senior Member, IEEE) received the B.Eng., M.Sc., and Ph.D. degrees in electrical engineering from Zhejiang University, Hangzhou, China, in 1996, 1999, and 2005, respectively.

Since 1999, she has been with the College of Electrical Engineering, Zhejiang University, where she is currently a Professor. Since 2019, she has also been a part-time Professor with the Lanzhou University of Technology, Lanzhou, China. Her research interests include analysis and control of linear machines, and permanent magnet machines.

Z. Q. Zhu (Fellow, IEEE) received the B.Eng. and M.Sc. degrees from Zhejiang University, Hangzhou, China, in 1982 and 1984, respectively, and the Ph.D. degree from the University of Sheffield, Sheffield, U.K., in 1991, all in electrical and electronic engineering.

Since 1988, he has been with the University of Sheffield, where since 2000, he has been a Professor with the Department of Electronic and Electrical Engineering. He is currently the Royal Academy of Engineering/Siemens Research Chair, and the Head of the Electrical Machines and Drives Research Group, the Academic Director of Sheffield Siemens Gamesa Renewable Energy Research Centre, the Director of CRRC Electric Drives Technology Research Centre, and the Director of Midea Electrical Machines and Control Systems Research Centres. His current major research interests include the design and control of permanent magnet machines and drives for applications ranging from electric vehicles through domestic appliance to renewable energy.

Dr. Zhu is the recipient of the 2021 IEEE Nikola Tesla Award and the 2019 IEEE IAS Outstanding Achievement Award. He is a Fellow of the Royal Academy of Engineering, U.K.